ROYAL SOCIETY
OF **CHEMISTRY**

PAPER
Björn K. Birdsong, Richard T. Olsson *et al.*
Flexible and fire-retardant silica/cellulose aerogel using
bacterial cellulose nanofibrils as template material

ROYAL SOCIETY
OF CHEMISTRY

Check for updates

Flexible and fire-retardant silica/cellulose aerogel using bacterial cellulose nanofibrils as template material†

Björn K. Birdsong,[*a] Qiong Wu, [ID] [a] Mikael S. Hedenqvist,[a] Antonio J. Capezza, [ID] [a] Richard L. Andersson,[a] Anna J. Svagan, [ID] [a] Oisik Das,[b] Rhoda Afriyie Mensah[b] and Richard T. Olsson [ID] [*a]

This study explores the possibility of using various silsesquioxane precursors such as (3-aminopropyl) triethoxysilane (APTES), methyltrimethoxysilane (MTMS), and tetraethyl orthosilicate (TEOS) to produce silsesquioxane-bacterial cellulose nanofibre (bCNF) aerogels. Each precursor allowed to customize the aerogel properties, leading to unique properties suitable for various applications requiring lightweight insulative materials. When utilizing APTES as the silsesquioxane precursor, an aerogel capable of over 90% recovery after compression was formed, making them suitable for flexible applications. When MTMS was used as the precursor, the aerogel retained some compression recovery (80%) but had the added property of superhydrophobicity with a contact angle over 160° due to the presence of CH_3 functional groups, enabling water-repellence. Finally, TEOS allowed for excellent thermal insulative properties with a low Peak Heat Release Rate (PHRR), making it a promising candidate for fire-resistant applications. The customization of these aerogel materials was attributed to a combination of the chemical composition of the silsesquioxane precursors and the morphology of the coated bacterial cellulose nanofibres (bCNF), such as CH_3 groups found in MTMS enabled for superhydrophobicity. Differences in morphology, such as uniform and smooth silsesquioxane coatings when using APTES or a "pearl-necklace" morphology using TEOS, enabled either compression recovery and flexibility or low thermal conduction. This investigation of silsesquioxane-bCNF provides a good understanding of the importance of the choice of precursor effect on insulating aerogel properties.

Introduction

Silica aerogels are highly porous materials derived from a sol–gel condensation reaction followed by supercritical drying.[1–3] Their interesting and unique properties, such as low density, high porosity, large surface area, and low thermal conductivity, make them super-efficient thermal insulators,[4] as catalyst supports[5] and dielectric materials.[6–8] However, despite silica aerogels demonstrating interesting and promising properties, there are major challenges related to their brittle and fragile nature,[9,10] in addition to expensive manufacturing.[6] In fact, most aerogels easily break into pieces and powder with the application of only a small amount of strain, typically smaller

than 10%.[11] One explanation for the fragile nature of these materials is the pearl-necklace-like structure of the silica network, consisting of 3 to 10 nm diameter spherical silica nanoparticles, where due to the smaller cross-section, the "neck" regions experience higher force, compared to the thicker "pearl" regions, and are therefore prone to cracks and breaking.[12] A similar pearl-necklace structure was recently, for the first time, obtained along the fibril of nanocellulose (CNF) by controlling the condensation of tetraethyl orthosilicates (TEOS) in aqueous suspension of CNFs.[13] The resulting hybrid cellulose/silica aerogel material showed new interesting properties such as a highly porous nature, improved fire safety properties, and increased thermal stability in regard to the cellulose component. Furthermore, it was possible to form the suspension into an aerogel while avoiding supercritical drying due to the mechanically supportive network of cellulose nanofibrils (CNF) stabilizing the aerogel during the freeze-drying.[13] However, similar to the Kistler aerogels (that use supercritical drying),[1] the materials were also very brittle and fragmented under small loads, *i.e.*, showing limited flexibility. A combination

ᵃ Department of Fiber and Polymer Technology, School of Chemical Science and Engineering, KTH Royal Institute of Technology, SE-100 44 Stockholm, Sweden. E-mail: birdsong@kth.se, rols@kth.se

ᵇ Department of Civil, Environmental and Natural Resources Engineering, Luleå University of Technology, 97187 Lulea, Sweden

† Electronic supplementary information (ESI) available. See DOI: https://doi.org/10.1039/d3ma01090b

of tetraethyl orthosilicate (TEOS) and trifunctional silsesquioxane precursor for the formation of less rigid silicone oxide networks was previously demonstrated as a useful method for the preparation of more flexible Kistler aerogels.[14–16] In fact, the use of only a trifunctional silsesquioxane precursor was shown to result in a significantly more flexible silicone oxide structure,[8,17,18] which have promoted copolymerization of the silica backbone with synthetic or natural polymeric compounds.[19–21] The solid network of these aerogels was always formed by replacing the reaction medium in the formed silica/silsesquioxane gel with liquid carbon dioxide (CO_2) under supercritical conditions.[22–26] From a practical perspective, supercritical drying is not only costly but also very elaborate and time-consuming as a result of the strict requirement of complete removal of any water remaining from the condensation of the silicone oxide network, which often demands repeated solvent exchange over extended times (3–4 days).[27] Additionally, there is always a risk with the high pressures involved in order to prevent collapse during the aerogels' preparation.[28,29] In light of the aformentioned, there is an urgent need to develop inexpensive and more efficient methods for aerogel preparation.

This article presents, for the first time, a robust flexible silica–cellulose aerogel prepared by *in situ* polymerization of various silsesquioxane precursors directly on the surface of the cellulose nanofibrils (CNFs), using simple freeze-drying to remove the liquid aqueous phase. The resulting materials demonstrated a transformation of properties from brittle to flexible, depending on the amount and type of different silica aerogel precursor used. At the same time, the hydrophilicity of the prepared hybrid aerogels could be varied from superhydrophobic with a contact angle exceeding 160° to completely hydrophilic. The flexible properties allowed the material to be bent and compressed with close to complete recovery. The different compositions of the silanes used as precursors for the silsesquioxane phases are discussed in terms of their ability to cover the CNF fibers uniformly and the reasons for their inability to deposit evenly from an aqueous solution. Due to the large-scale manufacturing of the precursors and the significant reduction of costs, avoiding supercritical drying, it is suggested that the materials have the potential to be upscaled on an industrial level.

Experimental

Materials

2-Propanol (reagent grade, ≥99.8%) was purchased from VWR, and Milli-Q water (MQw) (18.2 MΩ, pH = 7.0) was used as the aqueous medium. Tetraethyl orthosilicate (TEOS, ≥98%), ammonia hydroxide (aq. 28 wt%), (3-aminopropyl)triethoxysilane (APTES, ≥98%), methyltrimethoxysilane (MTMS, ≥95%) were purchased from Sigma-Aldrich and used as received. Bacterial cellulose (BC) was purchased from Monstra LLC (Thailand) as cubes with a volume of *ca.* 1 cm^3 and were grown from strains of Acetobacter Xylinum.

Purification of bacterial cellulose into bacterial nanofibers (bCNF) using acid hydrolysis

Bacterial cellulose nanofibers (bCNF) isolation followed the method developed by Hoogendoorn *et al.*, involving acid hydrolysis using

H_2SO_4.[30] An initial mass of 2 kg of bacterial cellulose (BC) cubes as received, was soaked for 5 days in Milli-Q® water (MQw) before treatment using 10 vol% NaOH at 100 °C for 10 min, followed by a 24 h water rinse to remove any impurities. The purified BC mass was blended into a slurry using a blender (Blendtec 625) and partially dewatered by pressing the slurry through a polyamide mesh (pore size: 46 μm, SEFAR). Acid hydrolysis was performed by adding the pure compressed BC mass into 1 liter of a 50 vol% H_2SO_4 solution heated to 60 °C, and acid hydrolysis occurred for 4 h under constant stirring (300 rpm) and 60 °C. Afterward, the slurry was quenched by the addition of 1 L of cold MQw. The hydrolyzed bCNF was washed thrice using centrifugation at 11 000 G for 10 min, with two intermediate supernatant exchanges with MQw. The resulting cellulose nanofibers (bCNF) dispersion was dialyzed for 22 days using dialysis tubing (MWCO = 100 kDa) until reaching a neutral pH at a final solid content of 0.87 wt%.

Silsesquioxane-coated cellulose nanofibrils

A dispersion of 3.6 mL (0.87 wt% bCNF) was mixed with 16.4 mL 2-propanol in a 50 mL polypropylene tube (see Fig. 1(a)). The bCNF suspension was ultrasonicated in an ultrasonic bath for 5 min at an average intensity of 300 W. The polypropylene tubes were mounted onto a vortex shaker (Vortex-Genie 1, US) and mixed for an additional 5 min before 126 μL, 252 μL, or 756 μL, (Low, Medium, and High) of the silsesquioxane precursor (APTES, MTMS, or TEOS), was added followed by another 5 min under vortex mixing. The condensation reaction was initiated by the addition of 63 μL, 123 μL, or 378 μL, respectively, aqueous ammonia hydroxide (aq. 28 wt%) followed by vortex mixing (maximum shaking) for 1 h under room temperature. Afterward, the dispersion (referred to as APTES-bCNF, MTMS-bCNF, and TEOS-bCNF) was washed of unreacted silsesquioxane precursors and isolated *via* centrifugation three times for 10 min at 6000 rpm using a (OHAUS FRONTIER 5706) centrifuge, and ethanol was used between each centrifugation cycle, before the material was finally being dispersed using MQw to 20 mL.

Aerogel casting

The dry aerogel materials were made by pouring 1.1 mL of the silsesquioxane-bCNF suspension into a 1.5 × 1.5 × 0.5 cm polypropylene mold before being placed on a cooled metal block immersed in liquid nitrogen (see Fig. 1(b)). The dispersion and mold were left to freeze for *ca.* 5 min before the frozen dispersion was removed from the mold and freeze-dried using a HyperCOOL (HCC-3110, Republic of Korea) freeze dryer. The dried aerogel materials were heat-treated using an oven (Memmert UNB 100) at 110 °C for 2 h before being stored in a desiccator with silica gel.

Characterization

Microscopy. The morphology of the aerogels was investigated using a field emission scanning electron microscope (FE-SEM; Hitachi S-4800, Japan). The samples were placed on a conductive carbon tape, and images were taken at an acceleration voltage between 1–3 kV and a current of 10 μA. The fibre
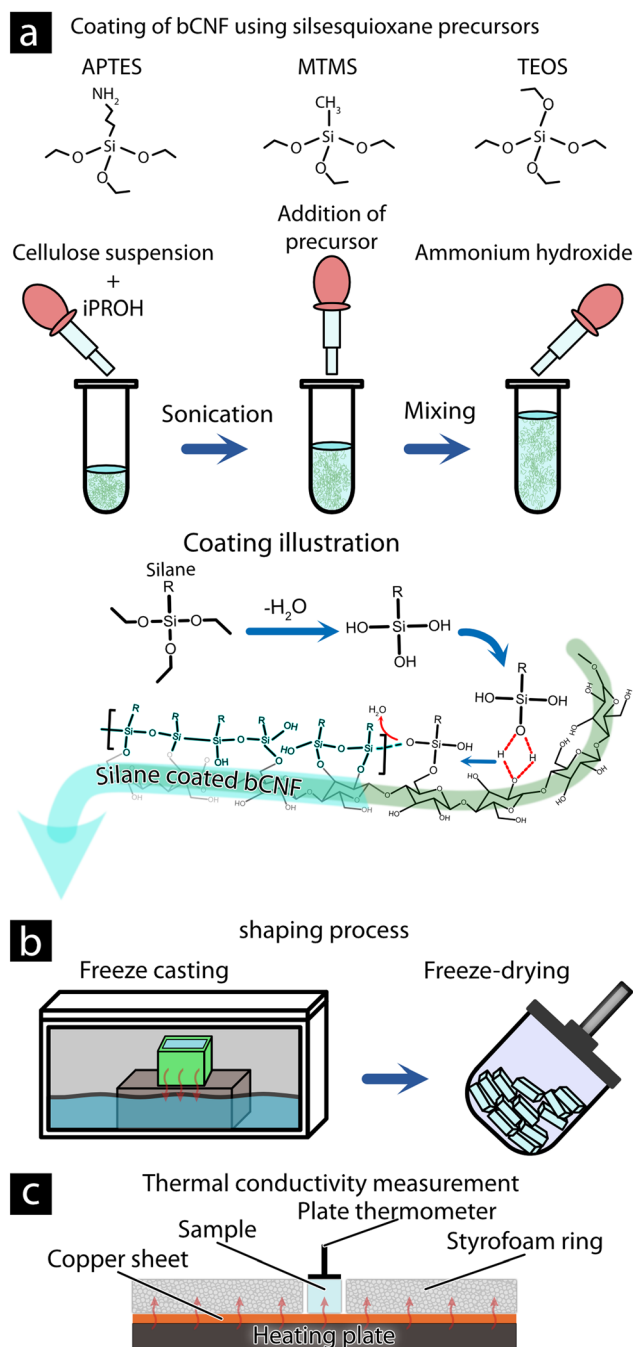
a Coating of bCNF using silsesquioxane precursors

APTES   MTMS   TEOS

Cellulose suspension + iPROH → Sonication → Addition of precursor → Mixing → Ammonium hydroxide

Coating illustration

Silane coated bCNF

b shaping process

Freeze casting → Freeze-drying

c Thermal conductivity measurement

Plate thermometer
Sample
Styrofoam ring
Copper sheet
Heating plate

Fig. 1 Illustration of the methodology for producing silsesquioxane-bCNF aerogel and methodology for thermal conductivity measurements. Coating reaction of bCNF *via* the addition of silsesquioxane precursors (a).[31,32] Aerogel shaping and drying procedure utilizing freeze casting and freeze-drying (b). Determination of thermal conductivity of aerogel materials (c).

thickness was determined by measuring the thickness of 50 randomly selected fibers using ImageJ[®], National Institutes of Health, Bethesda, Maryland, USA. Polarized optical microscopy (POM) was performed on aerogels using an inverted Axio vert. A1 Light Microscope (Carl Zeiss, Germany), equipped with cross-polarized light filters and a 10× magnification objective.

Fourier-transform infrared spectroscopy (FTIR). FTIR absorbance was measured on the freeze-dried aerogel materials and the freeze-dried bCNF using a PerkinElmer Spectrum 100, equipped with an ATR accessory, MIR TGS detector, and Specac golden gate with sapphire crystal. The measurements were performed with a resolution of 4 cm^{-1}, using 16 consecutive scans ranging from 600 to 4000 cm^{-1}.

Micro-scale combustion calorimetry (MCC). An MCC instrument from Fire Testing Technology (FTT) (United Kingdom) was used, following the standard in ASTM D7309, to evaluate the heat release properties of the aerogel materials and bCNF. Time and temperature to peak heat release rate were measured using a heating rate of 1 °C s^{-1} and a N_2/O_2 flow rate of 80/20 mL min^{-1}. The thermal oxidative degradation procedure (Method B) was used, wherein the samples were decomposed in a mixture of N_2 and O_2 at temperatures between 100 °C and 850 °C. Excess oxygen was added to force the volatiles/char to complete combustion at 900 °C.

Thermogravimetric analysis (TGA). To assess the thermal stability and SiO_x composition of the materials, thermogravimetric analysis (TGA) was performed. The TGA instrument used was a Mettler Toledo thermal analyzer (TGA/DSC 3+). 5–10 mg of the aerogel samples were placed in 70 μL alumina oxide (Al_2O_3) crucibles (ME-24123) and heated to 800 °C at a rate of 5 °C min^{-1} with a flow of 50 mL min^{-1} O_2.

Heat flow. The thermal conductivity of the materials was measured using a modified hot-plate method, similar to Blomfeldt *et al.*, seen in Fig. 1(c).[33] The sample was placed on a pre-heated, temperature-controlled hot plate with a polished copper metal sheet to hinder infrared radiation from the plate. A high thermal gradient of 11.8 K mm^{-1} was used to represent a closer resemblance to real-world conditions. A low thermal conductivity guard of HI 70 Styrofoam ring was placed on the copper sheet to prevent erroneous convection heating of the sample. To accurately measure the surface and sample temperature, the plate thermometer was allowed 10 min of heating before five measurements were done in 2-min intervals to obtain average temperatures used for the estimation of thermal conductivity (k) using eqn (1), where q is the effect of the heating plate (W), dy the thickness of the sample (mm), and dT the difference in temperature between the hot and cool side of the sample (K).[34]

$$k = -\frac{q\,\mathrm{d}y}{\mathrm{d}T} \tag{1}$$

Contact angle. The water-material contact angle, a measurement of surface wettability and hydrophilicity, was performed using a CAM200 contact angle meter (KSV Instruments, Finland) with an automatic dispenser and a CCD camera, and droplets of Milli-Q water. The static water contact angle was measured using the sessile drop technique. The tested aerogel was placed between two pre-cleaned micro slides and pressed using a 2 kg weight for 5 min, after which the films were heated to 110 °C for 2 h. Droplets of 4 μL volume were deposited on the films using a 200 μL pipette tip. Five measurements were

Paper

Materials Advances

conducted for each sample. All measurements were made at 23 ± 1 °C and $50 \pm 2\%$ RH. The photographic images of a water droplet in contact with the materials were taken for 40 s at 1% FPS; Software (Attension–Biolin Scientific) and the Young-Laplace method were used to calculate the contact angles.

Results and discussion

Compression and recovery of silsesquioxane-bCNF

Fig. 2(a), (c) and (e) shows the freeze-dried aerogels before, during, and after compression to *ca.* 50% of the original height. A clear difference in compression recovery can be seen when comparing the various materials. Both the APTES-bCNF and MTMS-bCNF aerogels show an almost complete recovery after the compression (*ca.* 94% and 81%, respectively, of original height), the TEOS-bCNF aerogel recovered significantly less (*ca.* 77% of original length). The recovery of the APTES-bCNF (High) and MTMS-bCNF (High) aerogels did not change significantly after being subjected to repeated compressions, differing only by 0–1%, while TEOS-bCNF (High) was only capable of *ca.* 54% recovery (see Fig. S1, ESI†). Light microscopy and high magnification SEM were used to investigate the cause of the different recovery capabilities. The resulting images seen in the optical microscope Fig. 2(b), (d) and (f) show that the overall structures of the aerogels do not differ significantly, containing both aligned and randomly oriented fibers (due to freezing). These macrostructure similarities suggest that they are not the reason for the difference in compression recovery. At higher magnification using SEM, differences in the coated fiber morphology can be observed (Fig. 2(b), (d) and (f), and Table 1). While the APTES-bCNF shows smooth uniform fibers aligned

in seemingly random directions, both the MTMS-bCNF and the TEOS-bCNF show the presence of secondary SiO_x structures in the form of spheres, reminiscent of SiO_2 spheres formed during the Stöber process.[35] The MTMS-bCNF seemed to divide into two regions, a relatively smooth and uniform fiber structure and SiO_x spheres nested between these fibers (see Fig. 2(d) high magnification). The same spherical structures can be seen in the TEOS-bCNF (Fig. 2(f) high magnification); however, in this case, they were no longer nested between the fibers but instead have formed a sort of "pearl-necklace" structure along the bCNF. These secondary SiO_x structures and the difference in coating smoothness were attributed to the observed difference in ductility and compression recovery, where non-uniform coating results in stress points on the fiber, leading to breaking.[36]

Surface composition of silsesquioxane coated bCNF

Fig. 3 shows the obtained FTIR spectra of the APTES, MTMS, TEOS-bCNF aerogels, and pure bCNF aerogel. From the spectra, signature peaks differentiate the coated bCNF aerogels from the pure bCNF aerogel. APTES-bCNF contains two clear peaks visible at 1560 cm^{-1} and 920 cm^{-1} corresponding to NH_2 bending/scissoring vibrations and Si–C vibrations, in addition a slight increase in intensity of C–H stretching vibrations can be observed at 2800–2950 cm^{-1}.[37,38] In comparison the spectra of MTMS coated bCNF shows distinct peaks at 1270 cm^{-1} and 760 cm^{-1} corresponding to $Si–CH_3$ stretching and Si–C stretching vibrations.[39,40] Lastly, the spectra belonging to TEOS-bCNF show instead one broad peak at 1053 cm^{-1} attributed to a combination of Si–O–Si stretching and vibrations and a slightly obscured peak at 950 cm^{-1} corresponding to Si–O–H stretching vibrations.[41]
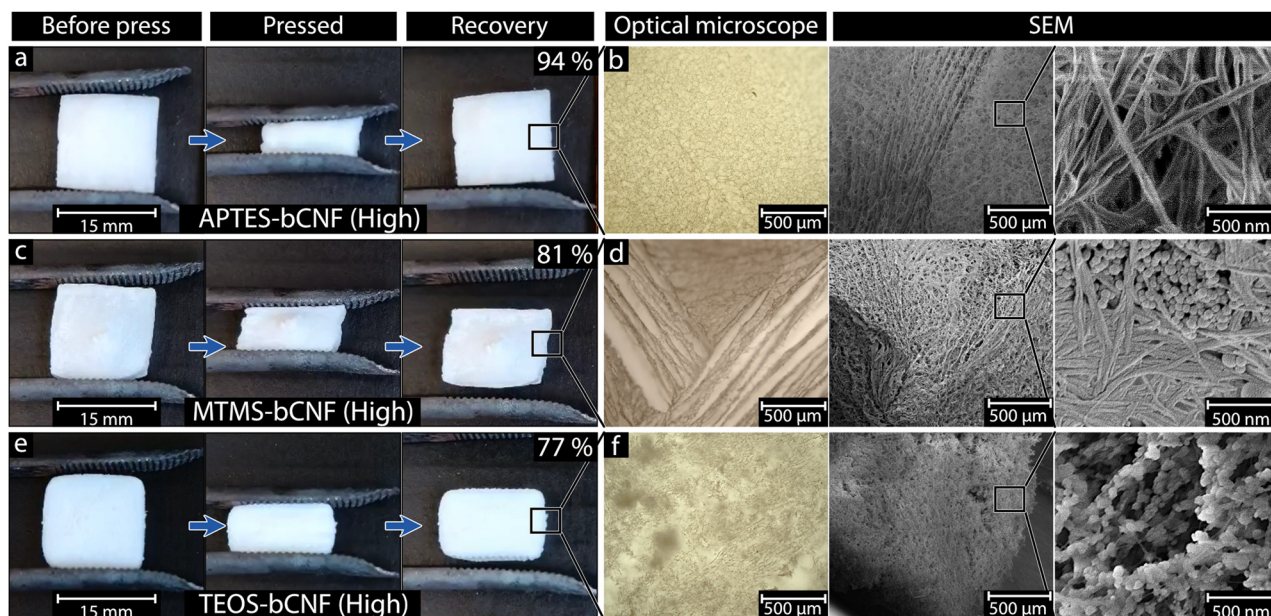

Fig. 2 Images of aerogel materials before, during, and after compression using "High" amount of APTES (a), MTMS (c), and TEOS (e). The aerogel structures were imaged using optical microscopy and SEM (b), (d), and (f).

Table 1 Aerogel fiber thickness depending on silsesquioxane precursor and the wall thickness of EPS 80 foam

Sample	Fiber thickness (nm)	Compression recovery (%)
bCNF	15 ± 4	—
APTES-bCNF (High)	51 ± 22	94
MTMS-bCNF (High)	38 ± 11	81
MTMS-bCNF (High) spheres	86 ± 29	—
TEOS-CNF (High)	21 ± 6	77
TEOS-CNF (High) spheres	86 ± 23	—
EPS 80 foam	296 ± 126	84

± indicates the standard deviation from a minimum of 50 measurements. For all thickness estimations, see Table S1 (ESI).
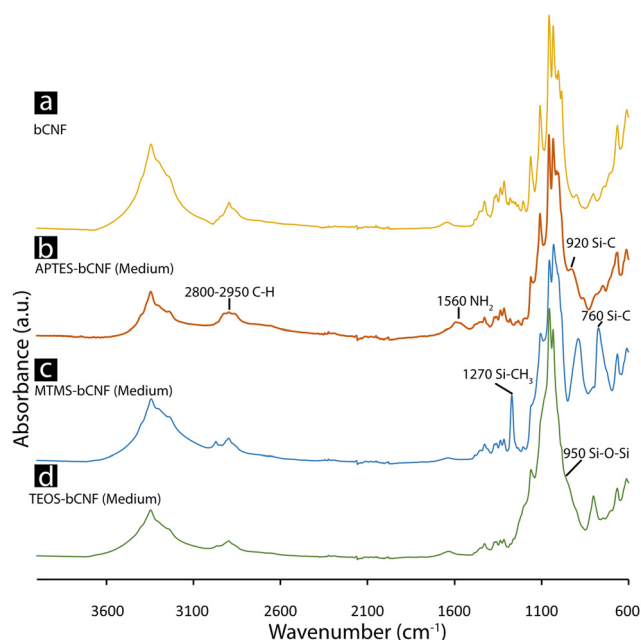
Fig. 3 FTIR spectra of the freeze-dried samples. bCNF (a), APTES-bCNF (Medium) (b), MTMS-bCNF (Medium) (c), and TEOS-bCNF (Medium) (d).

Insulation properties and comparison of silsesquioxane aerogels

Thermal conductivity, combustion, and thermal stability were investigated to assess the potential use of the aerogels for insulation. Fig. 4(a) shows the thermal conductivity (k) of the silsesquioxane-bCNF aerogels, with all materials ranging from 0.08 to 0.10 W m^{-1} K^{-1}, signifying that the aerogel materials exhibited low thermal conductivity regardless of chemical composition and coating morphology. Furthermore, as seen in Fig. 4(a), using higher amounts of the silsesquioxane precursor resulted in an overall decrease in thermal conductivity. The only exception was MTMS-bCNF (Medium), where the thermal conductivity saw a marginal (low significance) increase (0.095 W m^{-1} K^{-1}) in comparison to 0.093 W m^{-1} K^{-1} for MTMS-bCNF (Low). However, when comparing MTMS-bCNF (Low) to MTMS-bCNF (High) (0.087 W m^{-1} K^{-1}), a much clearer trend in the same direction as the other silsesquioxane-bCNF aerogels was observed. Additionally, as shown in Table 2, the

density of the silsesquioxane-bCNF aerogels increased with higher amounts of precursor, implying that the lower thermal conductivity was inversely proportional to the material's density. This non-intuitive relationship can be explained by way of the higher-density materials having less space between the solid structures in the aerogel, leading to a restriction of the mean path for the gas molecules inside the aerogel cell, lowering the thermal conductivity of the gas inside the cells, reminiscent of the Knudsen effect, often observed in low thermal conductivity aerogels.[42] In addition, any convection inside the aerogel cells is also restricted by similar logic. The difference in density was proposed to stem from both the coating morphology of bCNF and the secondary silsesquioxane structures shown in Fig. 2(b), (d) and (f), scanning electron micrographs. The structural differences of the aerogel, with the addition of the secondary silsesquioxane structures, may additionally contribute to a decrease in cell size, leading to an increased Knudsen effect as well as decreased gas diffusion through the aerogels.[43] The thermal conductivity obtained using the modified hot plate method in this work typically yields higher values of thermal conductivities compared to other methods, as it relies on relatively large thermal gradients where, *e.g.*, internal thermal radiation may have a bigger influence, similar to real-world conditions. When EPS 80 was measured using the same method, a value of 0.094 W m^{-1} K^{-1} was obtained, which is *ca.* 2.5 times higher than values obtained from the manufacturer at 0.038 W m^{-1} K^{-1}.[44] Using this comparison, it was assumed that the thermal conductivity of the silsesquioxane-bCNF's could be much lower under different conditions, indicating that the thermal conductivity of the bCNF aerogels could approach the thermal conductivity of classical aerogels reported in literature (*ca.* 0.003 W m^{-1} K^{-1}).[45]

Fire retardant properties

Microscale combustion calorimetry (MCC) was used to validate whether the aerogels were viable for building insulation or use in other insulation areas where fire-safe properties are important. A critical factor to consider in fire safety is the time to peak heat release rate (tPHRR), allowing for an estimation of time before a fire intensifies out of control.[46] Additionally, the peak heat release rate (PHRR), indicating the highest point in a burning material's heat release rate curve, is one of the most important parameters to gauge fire safety.[47,48] Fig. 4(b) shows that although the tPHRR was similar between the various aerogels ranging between 240 to 260 s, the PHRR varied significantly for the aerogel materials, ranging from an average PHRR of *ca.* 377 W g^{-1} after *ca.* 250 s for APTES-bCNF, *ca.* 173 W g^{-1} after *ca.* 245 s for MTMS-bCNF, and only *ca.* 33 W g^{-1} after *ca.* 257 s for TEOS-bCNF (see Fig. S2a, ESI† for all PHRR values), yet remained comparable in PHRR to other reported aerogels.[49] It was suggested that the reason for the significant differences in PHRR between the various aerogels was due to the fractional chemical composition of the various silanes, where APTES increased the amount of combustible material in the form of three CH$_2$ and one NH$_3$ for every APTES reacted. In the case of MTMS-bCNF, a single CH$_3$ is added per attached
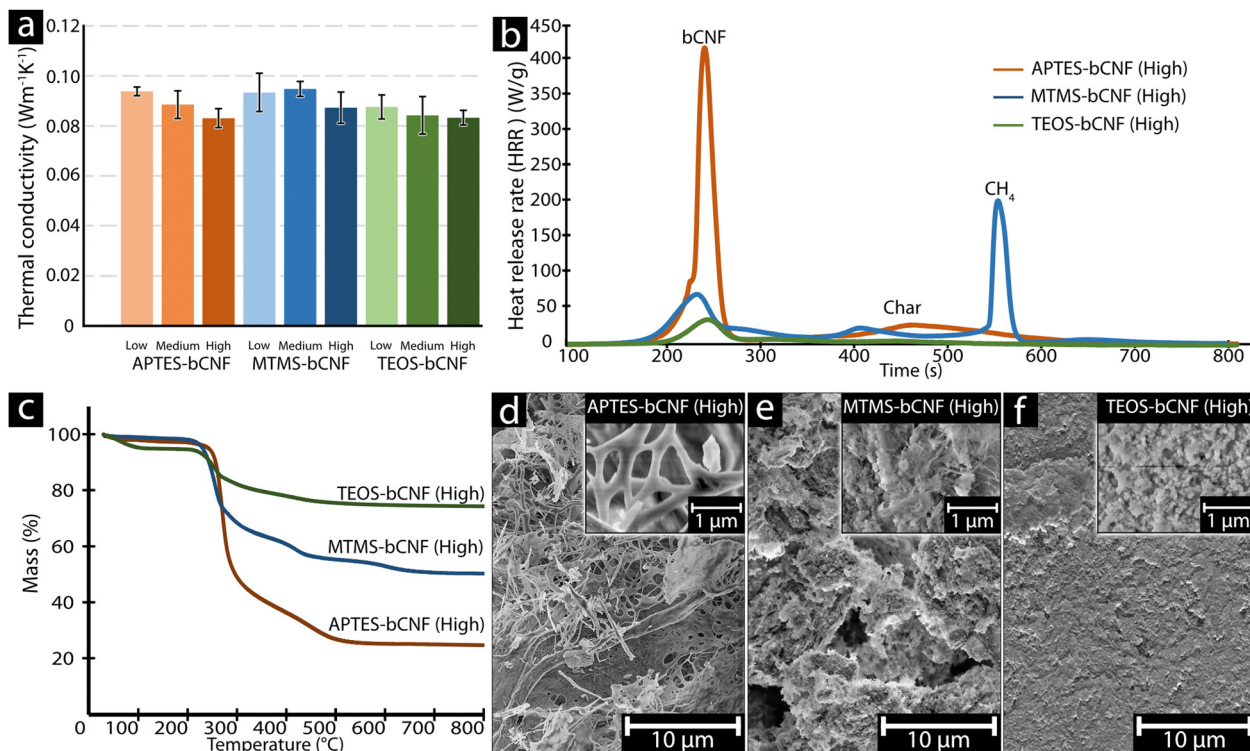
Fig. 4 Thermal conductivity of materials was measured using a plate thermometer using the setup seen in Fig. 1(c) (a). Microscale combustion calorimetry (b), thermogravimetrically analysis (TGA) (c), and SEM images of the high-concentration silenized materials after TGA treatment (d)–(f).

Table 2 Measured densities of aerogel materials

Density (kg m^{-3})								
APTES-bCNF			MTMS-bCNF			TEOS-bCNF		
Low	Medium	High	Low	Medium	High	Low	Medium	High
1.9 ± 0.1	2.2 ± 0.1	2.5 ± 0.1	1.3 ± 0.1	1.6 ± 0.1	3.0 ± 0.1	1.5 ± 0.1	2.4 ± 0.1	8.5 ± 0.1

Density values were obtained by weighing virgin aerogel with a known volume.

silane, resulting in less combustible material per gram compared to APTES-bCNF; this was even more pronounced in the case of TEOS-bCNF as no additional combustible material was added. Fig. S2a (ESI†) confirms this trend further by showing that the greater the amount of APTES used, the higher the PHRR was, contrary to MTMS and TEOS when there was a clear decrease in PHRR when higher amounts of silsesquioxane precursor were used. Additionally, regardless of the silsesquioxane precursor used or amount, no significant change in tPHRR was observed compared to the pure bCNF, suggesting that the initial peak (*ca.* 261 seconds) was gasification of bCNF, followed by combustion of residual char between 400 to 500 °C, and finally in the case of MTMS-bCNF conversion of Si–CH$_3$ into an imperfect Si–C network (*ca.* 590 °C) (Fig. 4(b) and Fig. S3, ESI†).[50,51] When comparing the aerogel materials to commercial insulation materials such as EPS 80 foam, it was clear that even the worst aerogel with regards to PHRR (APTES-bCNF (High)) had approximately 3 times lower PHRR in comparison to the EPS 80 foam (*ca.* 1160 W g^{-1}).[52] The large difference in

PHRR between the conventional EPS 80 foam and the aerogel materials demonstrates that the aerogel materials, regardless of composition, were safer from a fire safety perspective, further emphasized in a candle ignition test (see Fig. S4, ESI† and additional videos attached), where it was clear that even though the aerogel materials ignited, the burn time was significantly shorter and contributed with less heat.

Fig. 4(c) shows the thermal decomposition of the silsesquioxane-bCNF aerogels using thermogravimetric analysis (TGA) to determine the material's thermal stability and SiO$_x$ content. It was found that regardless of the silane used for the coating, the aerogels exhibited similar thermal degradation behavior. There was a small mass loss between 30–200 °C for all the samples, which was attributed to water removal. The difference in moisture removal between the various silsesquioxane-bCNF's where TEOS-bCNF had a more pronounced decrease in mass (*ca.* 5 wt%) at 30–200 °C compared to the other APTES and MTMS-bCNF (*ca.* 2–1.5 wt%). It was suggested that this was due to the hydrophilicity of TEOS, leading to

greater moisture adsorption from the air. The second mass loss occurred for all aerogels between 220–300 °C, characteristic of the thermal degradation of cellulose.[53–55] Both APTES-bCNF and MTMS-bCNF shared an additional mass loss between *ca.* 350 and 450 °C attributed to the decomposition of amino groups and the evolution of methanol from the CH_3 groups, respectively.[51,56] Lastly, a third mass loss can be observed for MTMS-bCNF at *ca.* 600 °C highly similar to the combustion observed in MCC (Fig. 4(b)) and was again attributed to the thermal removal of CH_3.[51,57] The difference in the remaining final mass was attributed to the cellulose to SiO_x ratio, where the more reactive silanes (MTMS and TEOS) where able to not only coat the cellulose fiber's with thicker layers but also produce secondary SiO_x structures (see Fig. 2(d), (f) and 4(e), (f)), which where thermally stable. Lastly, it was possible to estimate the SiO_x content of the various aerogels from the residual mass, where APTES-bCNF only resulted in *ca.* 24.7 wt% SiO_x, MTMS *ca.* 50.4 wt% SiO_x, and TEOS-bCNF *ca.* 74.3 wt% SiO_x.

Fig. 4(d)–(f) shows SEM images of the remaining aerogel materials after TGA analysis ending at 800 °C. Comparing the materials seen in Fig. 4(d)–(f) with the materials seen in Fig. 2(b), (d) and (f), it is clear that the overall morphology of the materials remains intact, and where the structural differences between APTES, MTMS, and TEOS-bCNF remain distinct. Fig. 4(d) shows that the APTES-bCNF has kept the long fibrous structures; however, larger agglomerates are also seen, which at higher magnification are seen to be composed of smaller fibers. Similarly, MTMS-bCNF retained the two distinct structures seen previously in Fig. 2(d) with both fibers and spherical particles visible. Lastly, TEOS-bCNF shows only spherical particles that are lumped together to some degree, similar to the TEOS-bCNF seen in Fig. 2(f) and more conventional TEOS-based aerogels.[58]

Investigation of hydrophilicity of silsesquioxane-bCNF

Since MTMS is well documented to have hydrophobic properties and the ability to make coated materials hydrophobic, contact angle (CA) was used to investigate the hydrophilicity of the silsesquioxane-bCNF.[59] Fig. 5 shows the measured contact angles for the aerogel materials after being pressed using a 2 kg weight for 5 min; the motivation for the pressing procedure was to minimize the contribution of surface roughness on wettability and to measure on a flat surface for improved measurement accuracy. Non-pressed aerogels were also investigated to further compare the effect of the surface morphology and roughness on wettability (Fig. S5, ESI†). This showed that the non-pressed APTES-bCNF and MTMS-bCNF aerogels, regardless of silane amount used, achieved hydrophobicity with contact angles well above 90° while the TEOS-bCNF aerogels, however, remained hydrophilic. The hydrophobicity seen in APTES-bCNF and MTMS-bCNF was suggested to be in part caused by the high surface roughness found in the aerogel materials but not enough to overcome the highly hydrophilic surface formed from the TEOS precursor.[60–63] As seen in Fig. 5, the only material exhibiting low wettability after pressing was MTMS-bCNF (High) (Fig. 5(a)), even exceeding the hydrophobic
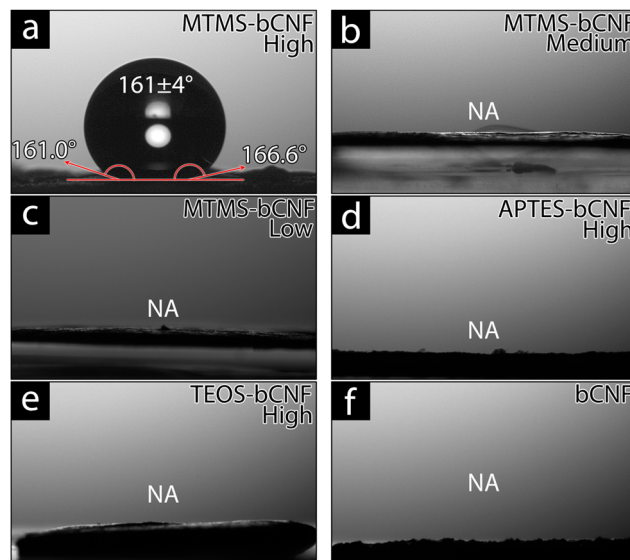

Fig. 5 Water contact angle of pressed aerogel materials.

EPS 80 foam material (Fig. S5(i), ESI†), while all other pressed aerogels completely absorbed the 4 μL MQw droplet in less than 5 s. Although MTMS-bCNF shares structural morphology with both APTES-bCNF and TEOS-bCNF, it was unique regarding wettability. Being comprised of both smooth uniformly coated bCNF (shared with APTES-bCNF) and spherical silsesquioxane structures (shared with TEOS-bCNF), yet remained superhydrophobic suggests that it was not the morphology of the coating on the bCNF, but rather the chemical composition (see Fig. 1(a)) of the exposed surface and the surface energy of the material that affected the contact angle.[64,65] While MTMS-bCNF (High) exhibited exceptional superhydrophobicity, with a contact angle of $161 \pm 4°$, well above the minimum CA needed to be considered superhydrophobic (150°), contrary, MTMS-bCNF (Low and Medium) did not show any hydrophobicity, instead absorbing the MQw as quickly as the other materials. It was suggested that this was due to an incomplete silsesquioxane network forming on the bCNF, leading to the presence of OH groups on the bCNF fiber remaining exposed, or that there was a minimum coverage of CH_3 groups needed to achieve hydrophobicity.[66,67] In contrast, the functional groups present in APTES-bCNF (NH_2) and TEOS-bCNF (OH) are both hydrophilic, resulting in a hydrophilic behavior regardless of the amount of the silsesquioxane precursor used.[68,69] Interestingly, all materials were hydrophilic without the 110 °C 2 h heating, suggesting that the presence of hard-bound moisture in the aerogels significantly affects the material's wettability.

Silsesquioxane precursor amount effect on coatings

In this study, various amounts of silsesquioxane precursors were used to investigate the effect of silane abundance on coating morphology and the final chemical composition of the aerogel materials. The morphology of the coated bCNF was shown to vary to some degree depending on the amount and type of silane used. As seen in Table S1 (ESI†), there was

little difference in the APTES-bCNF thickness ranging from 46–59 nm and no difference in coating morphology regardless of the amount of APTES used. Furthermore, although both MTMS and TEOS silanized-bCNF shared this relatively uniform fiber thickness regardless of the amount of silane used, ranging from ca. 20–38 nm for MTMS-bCNF and ca. 21–31 for TEOS-bCNF, the morphologies of these materials were affected by the silane amount. When high amounts of MTMS were used, the morphology of the silsesquioxane coatings changed from smooth and uniform coatings, similar to the APTES coatings, into a two-phase system, as shown in Fig. 2(d). In the case of TEOS, the only observable difference in morphology was the size and amount of the silsesquioxane spheres observed (see Table S1, ESI† how the material deposited as secondary particles). Lastly, it was determined from TGA that regardless of the amount of silane used, the amount of silsesquioxane remained relatively unchanged when APTES was used; in contrast, for MTMS and TEOS a significant increase in silsesquioxane present when using a higher amount of precursor, as seen in Fig. S6 (ESI†), suggesting that APTES reaches a coating maximum with a relatively low amount, while both MTMS and TEOS continues to increase the amount of silsesquioxane material present, deposited in the form of secondary particles.

Conclusions

The possibility of producing various silsesquioxane-bCNF aerogels, achieved through the use of different silsesquioxane precursors, namely APTES, MTMS, and TEOS, was demonstrated in this study. The choice of silsesquioxane precursor allowed for the customization of the coating morphology on the bCNF, varying from uniform, smooth coatings when using APTES to a mix of both smooth uniform fiber coatings and secondary spherical SiO_x particles using MTMS and a unique "pearl-necklace" structures along the bCNF when TEOS was used. These coating morphologies are suspected of having given rise to the various compression recovery behaviors, where APTES-bCNF demonstrated the best compressibility recovery (ca. 94% recovery) followed by MTMS-bCNF and TEOS-bCNF (ca. 81 and 77%). Despite the high compression recovery, the aerogel materials remained much less dense in comparison to other mechanically stable foam materials, such as Styrofoam, ranging from only 1.6 to 8.5 kg m^{-3}.

The surface composition of the silsesquioxane-bCNF was shown to have a dramatic effect on the hydrophilicity of the pressed aerogels, where only MTMS-bCNF (High) exhibited hydrophobicity ($>160°$), which was attributed to the abundance of CH_3 functional groups present on the surface of the material. In contrast, regardless of the amount of APTES or TEOS used, the APTES-bCNF and TEOS-bCNF pressed aerogels always exhibited hydrophilicity.

Lastly, the thermal properties of the aerogel materials were investigated using TGA and MCC, revealing that the composition of the silsesquioxane-bCNF aerogels varied from ca. 25 wt% SiO_x (APTES-bCNF) to 74 wt% SiO_x (TEOS-bCNF). This difference in

SiO_x content was attributed to the large difference in peak heat release rate (PHRR), where APTES-bCNF had a PHRR increase of ca. 74% while MTMS-bCNF and TEOS-bCNF had a PHRR decrease of ca. 71 and 86% respectively. The drastic decrease in PHRR for MTMS-bCNF and TEOS-bCNF combined with the low thermal conductivity (0.08–0.10 W m^{-1} k^{-1} in high thermal gradients, and approaching 0.04 W m^{-1} K^{-1} in other conditions) makes them promising candidates as insulation materials for fire-resistant insulation applications.

Author contributions

B. K. B. carried out all laboratory experiments included in this study. B. K. B. also performed all characterizations. B. K. B. and R. T. O. wrote the manuscript, with Q. W. writing the introduction. O. D. and R. A. M. helped interpret MCC data and provided interpretation of MCC data. M. H., R. L. A., and A. J. S. reviewed thermal conductivity data and provided input on improvements. A. J. C., M. H., and R. T. O. reviewed the manuscript, with R. T. O., recognizing the concept of using cellulose nanofibers as a template material for silsesquioxane aerogels.

Conflicts of interest

There are no conflicts to declare.

Acknowledgements

Notes and references

1 S. S. Kistler, Coherent Expanded Aerogels and Jellies, *Nature*, 1931, **127**, 741, DOI: **10.1038/127741a0**.
2 S. J. Teichner, G. A. Nicolaon, M. A. Vicarini and G. E. E. Gardes, Inorganic oxide aerogels, *Adv. Colloid Interface Sci.*, 1976, **5**, 245–273, DOI: **10.1016/0001-8686(76)80004-8**.
3 S. S. Kistler, Coherent Expanded-Aerogels, *J. Phys. Chem.*, 1932, **36**, 52–64, DOI: **10.1021/j150331a003**.
4 J. Fricke, *et al.*, *Therm. Conduct.*, 1990, **21**(21), 235–245.
5 G. M. Pajonk, Some catalytic applications of aerogels for environmental purposes, *Catal. Today*, 1999, **52**, 3–13, DOI: **10.1016/S0920-5861(99)00057-7**.
6 M. A. Aegerter, N. Leventis and M. M. Koebel, *Advances in sol–gel derived materials and technologies (En ligne)*, Springer Science + Business Media, LLC New York, New York, 2011.
7 G. M. Pajonk, Aerogel catalysts, *Appl. Catal.*, 1991, **72**, 217–266, DOI: **10.1016/0166-9834(91)85054-Y**.
8 S. D. Bhagat, C.-S. Oh, Y.-H. Kim, Y.-S. Ahn and J.-G. Yeo, Methyltrimethoxysilane based monolithic silica aerogels via ambient pressure drying, *Microporous Mesoporous Mater.*, 2007, **100**, 350–355, DOI: **10.1016/j.micromeso.2006.10.026**.

9 H. Yu, X. Liang, J. Wang, M. Wang and S. Yang, Preparation and characterization of hydrophobic silica aerogel sphere products by co-precursor method, *Solid State Sci.*, 2015, **48**, 155–162, DOI: **10.1016/j.solidstatesciences.2015.08.005**.

10 H. Maleki, L. Durães and A. Portugal, An overview on silica aerogels synthesis and different mechanical reinforcing strategies, *J. Non-Cryst. Solids*, 2014, **385**, 55–74, DOI: **10.1016/j.jnoncrysol.2013.10.017**.

11 K. E. Parmenter and F. Milstein, Mechanical properties of silica aerogels, *J. Non-Cryst. Solids*, 1998, **223**, 179–189, DOI: **10.1016/S0022-3093(97)00430-4**.

12 J. P. Randall, M. A. B. Meador and S. C. Jana, Tailoring Mechanical Properties of Aerogels for Aerospace Applications, *ACS Appl. Mater. Interfaces*, 2011, **3**, 613–626, DOI: **10.1021/am200007n**.

13 D. Liu, *et al.*, Cellulose nanofibril core–shell silica coatings and their conversion into thermally stable nanotube aerogels, *J. Mater. Chem. A*, 2015, **3**, 15745–15754, DOI: **10.1039/C5TA03646A**.

14 P. R. Aravind, P. Niemeyer and L. Ratke, Novel flexible aerogels derived from methyltrimethoxysilane/3-(2,3-epoxypropoxy)propyltrimethoxysilane co-precursor, *Microporous Mesoporous Mater.*, 2013, **181**, 111–115, DOI: **10.1016/j.micromeso.2013.07.025**.

15 A. V. Rao, M. M. Kulkarni, G. M. Pajonk, D. P. Amalnerkar and T. Seth, Synthesis and Characterization of Hydrophobic Silica Aerogels Using Trimethylethoxysilane as a Co-Precursor, *J. Sol-Gel Sci. Technol.*, 2003, **27**, 103–109, DOI: **10.1023/A:1023765030983**.

16 Y. U. W.-J. F. M.-H. H. E. X.-D. L. I. M.-W. He Fei, An Overview on Silica Aerogels Synthesized by Siloxane Co-precursors, *J. Inorg. Mater.*, 2015, **30**, 1243–1253.

17 A. Venkateswara Rao, S. D. Bhagat, H. Hirashima and G. M. Pajonk, Synthesis of flexible silica aerogels using methyltrimethoxysilane (MTMS) precursor, *J. Colloid Interface Sci.*, 2006, **300**, 279–285, DOI: **10.1016/j.jcis.2006.03.044**.

18 D. Y. Nadargi, S. S. Latthe, H. Hirashima and A. V. Rao, Studies on rheological properties of methyltriethoxysilane (MTES) based flexible superhydrophobic silica aerogels, *Microporous Mesoporous Mater.*, 2009, **117**, 617–626, DOI: **10.1016/j.micromeso.2008.08.025**.

19 H. Maleki, L. Durães and A. Portugal, Synthesis of lightweight polymer-reinforced silica aerogels with improved mechanical and thermal insulation properties for space applications, *Microporous Mesoporous Mater.*, 2014, **197**, 116–129, DOI: **10.1016/j.micromeso.2014.06.003**.

20 N. Leventis, A. Sadekar, N. Chandrasekaran and C. Sotiriou-Leventis, Click Synthesis of Monolithic Silicon Carbide Aerogels from Polyacrylonitrile-Coated 3D Silica Networks, *Chem. Mater.*, 2010, **22**, 2790–2803, DOI: **10.1021/cm903662a**.

21 M. Meador, L. Capadona, L. McCorkle, D. Papadopoulos and N. Leventis, Structure−Property Relationships in Porous 3D Nanostructures as a Function of Preparation Conditions: Isocyanate Cross-Linked Silica Aerogels, *Chem. Mater.*, 2007, **19**, 2247–2260, DOI: **10.1021/cm070102p**.

22 A. Demilecamps, G. Reichenauer, A. Rigacci and T. Budtova, Cellulose–silica composite aerogels from "one-pot" synthesis, *Cellulose*, 2014, **21**, 2625–2636, DOI: **10.1007/s10570-014-0314-3**.

23 A. Demilecamps, C. Beauger, C. Hildenbrand, A. Rigacci and T. Budtova, Cellulose–silica aerogels, *Carbohydr. Polym.*, 2015, **122**, 293–300, DOI: **10.1016/j.carbpol.2015.01.022**.

24 J. C. H. Wong, H. Kaymak, P. Tingaut, S. Brunner and M. M. Koebel, Mechanical and thermal properties of nano-fibrillated cellulose reinforced silica aerogel composites, *Microporous Mesoporous Mater.*, 2015, **217**, 150–158, DOI: **10.1016/j.micromeso.2015.06.025**.

25 A. C. Pierre and G. M. Pajonk, Chemistry of Aerogels and Their Applications, *Chem. Rev.*, 2002, **102**, 4243–4266, DOI: **10.1021/cr0101306**.

26 D. J. Boday, *et al.*, Strong, Low-Density Nanocomposites by Chemical Vapor Deposition and Polymerization of Cyanoacrylates on Aminated Silica Aerogels, *ACS Appl. Mater. Interfaces*, 2009, **1**, 1364–1369, DOI: **10.1021/am900240h**.

27 D. B. Mahadik, Y. K. Lee, N. K. Chavan, S. A. Mahadik and H.-H. Park, Monolithic and shrinkage-free hydrophobic silica aerogels via new rapid supercritical extraction process, *J. Supercrit. Fluids*, 2016, **107**, 84–91, DOI: **10.1016/j.supflu.2015.08.020**.

28 G. Carlson, D. Lewis, K. McKinley, J. Richardson and T. Tillotson, Aerogel commercialization: technology, markets and costs, *J. Non-Cryst. Solids*, 1995, **186**, 372–379, DOI: **10.1016/0022-3093(95)00069-0**.

29 F. Schwertfeger, D. Frank and M. Schmidt, Hydrophobic waterglass based aerogels without solvent exchange or supercritical drying, *J. Non-Cryst. Solids*, 1998, **225**, 24–29, DOI: **10.1016/S0022-3093(98)00102-1**.

30 B. W. Hoogendoorn, *et al.*, Cellulose nanofibers (CNFs) in the recycling of nickel and cadmium battery metals using electrodeposition, *Nanoscale Adv.*, 2023, **5**, 5263–5275, DOI: **10.1039/D3NA00401E**.

31 B.-F. Guo, *et al.*, Hydrosilylation Adducts to Produce Wide-Temperature Flexible Polysiloxane Aerogel under Ambient Temperature and Pressure Drying, *Small*, 2023, 2309272, DOI: **10.1002/smll.202309272**.

32 Y.-X. Qu, *et al.*, Facile synthesis of mechanically flexible and superhydrophobic silicone aerogels with tunable pore structure for efficient oil-water separation, *Mater. Today Chem.*, 2022, **26**, 101068, DOI: **10.1016/j.mtchem.2022.101068**.

33 T. O. J. Blomfeldt, *et al.*, Thermal Conductivity and Combustion Properties of Wheat Gluten Foams, *ACS Appl. Mater. Interfaces*, 2012, **4**, 1629–1635, DOI: **10.1021/am2017877**.

34 R. B. Bird, W. E. Stewart and E. N. Lightfoot, *Transport Phenomena*, Wiley, 2006.

35 W. Stöber, A. Fink and E. Bohn, Controlled growth of monodisperse silica spheres in the micron size range, *J. Colloid Interface Sci.*, 1968, **26**, 62–69, DOI: **10.1016/0021-9797(68)90272-5**.

36 P. Lee and T. Yano, The influence of fiber coating conditions on the mechanical properties of alumina/alumina composites, *Compos. Interfaces*, 2004, **11**, 1–13, DOI: **10.1163/156855404322681019**.

37 D. Liu, et al., Morphology and properties of silica-based coatings with different functionalities for Fe_3O_4, ZnO and Al_2O_3 nanoparticles, RSC Adv., 2015, 5, 48094–48103, DOI: 10.1039/c5ra04452a.

38 T. Oh, Comparison Between SiOC Thin Film by Plasma Enhance Chemical Vapor Deposition and SiO2 Thin Film by Fourier Transform Infrared Spectroscopy, J. Korean Phys. Soc., 2010, 56, 1150–1155, DOI: 10.3938/jkps.56.1150.

39 M. Lo, et al., Nanoscale Chemical-Mechanical Characterization of Nanoelectronic Low-k Dielectric/Cu Interconnects, ECS J. Solid State Sci. Technol., 2016, 5, P3018–P3024, DOI: 10.1149/2.0041604jss.

40 X. Wang, et al., Facile preparation of mechanically strong polyvinyl alcohol/MTMS aerogel composites with improved thermal stability, J. Nanopart. Res., 2021, 23, 261, DOI: 10.1007/s11051-021-05372-5.

41 Y.-K. Lv, An Imprinted Organic-Inorganic Hybrid Sorbent for Selective Separation of Cadmium from Aqueous Solution, Anal. Chem., 2004, 76, 453–457, DOI: 10.1021/ac0347718.

42 K. Malek and M.-O. Coppens, Knudsen Self- and Fickian Diffusion in Rough Nanoporous Media, J. Chem. Phys., 2003, 119(5), 2801–2811, DOI: 10.1063/1.1584652.

43 H. Zhang, et al., Experimental Characterization of the Thermal Conductivity and Microstructure of Opacifier-Fiber-Aerogel Composite, Molecules, 2018, 23, 2198, DOI: 10.3390/molecules23092198.

44 Bewi. BP-21-10-04-EN-EPS-80_2021_10_05, https://bewi.com/wp-content/uploads/2023/02/BP-21-10-04-EN-EPS-80_2021_10_05.pdf (2021).

45 D. R. Lide, ed. W. M. Haynes, Handbook of chemistry and physics 95 edition, Section 12, CRC Press, Boca Raton (FL), 2015, vol. 226.

46 J. H. Troitzsch, Fires, statistics, ignition sources, and passive fire protection measures, J. Fire Sci., 2016, 34, 171–198, DOI: 10.1177/0734904116636642.

47 R. A. Mensah, et al., A review of sustainable and environment-friendly flame retardants used in plastics, Polym. Test., 2022, 108, 107511, DOI: 10.1016/j.polymertesting.2022.107511.

48 L.-Y. Lv, et al., Smart fire-warning materials and sensors: Design principle, performances, and applications, Mater. Sci. Eng., R, 2022, 150, 100690, DOI: 10.1016/j.mser.2022.100690.

49 H.-Y. Chen, et al., Facile fabrication of low-content surface-assembled MXene in silicone rubber foam materials with lightweight, wide-temperature mechanical flexibility, improved flame resistance and exceptional smoke suppression, Composites, Part A, 2024, 177, 107907, DOI: 10.1016/j.compositesa.2023.107907.

50 X. Wu, et al., Flame retardant polyurethane sponge/MTMS aerogel composites with improved mechanical properties under ambient pressure drying, J. Nanopart. Res., 2020, 22, 221, DOI: 10.1007/s11051-020-04958-9.

51 V. S. Smitha, P. M. A. Azeez, K. G. Warrier, B. N. Nair and U. N. S. Hareesh, Transparent and Hydrophobic MTMS/

52 M. McLaggan, K. Wilkens Flecknoe-Brown, A. Dragsted and P. Van Hees, Heat release and flame spread assessment of insulation in External Thermal Insulation Composite System (ETICS) façades, J. Phys.: Conf. Ser., 2018, 1107, 032021, DOI: 10.1088/1742-6596/1107/3/032021.

53 L. Yeng, M. U. Wahit and N. Othman, Thermal and flexural properties of regenerated cellulose(RC)/poly(3-hydroxy-butyrate)(PHB)biocomposites, J. Teknol., 2015, 75, 11, DOI: 10.11113/jt.v75.5338.

54 A. Bekatorou, et al., Bacterial Cellulose Production Using the Corinthian Currant Finishing Side-Stream and Cheese Whey: Process Optimization and Textural Characterization, Foods, 2019, 8, 193, DOI: 10.3390/foods8060193.

55 S. Torgbo and P. Sukyai, Biodegradation and thermal stability of bacterial cellulose as biomaterial: The relevance in biomedical applications, Polym. Degrad. Stab., 2020, 179, 109232, DOI: 10.1016/j.polymdegradstab.2020.109232.

56 E. P. Nhavene, G. F. Andrade, J. A. Faria, D. A. Gomes and E. M. Sousa, Biodegradable Polymers Grafted onto Multifunctional Mesoporous Silica Nanoparticles for Gene Delivery, ChemEngineering, 2018, 2, 24.

57 Y. Li, et al., Temperature dependence of dynamic mechanical behaviors in low density MTMS-derived silica aerogel, J. Porous Mater., 2018, 25, 4, DOI: 10.1007/s10934-017-0533-8.

58 A. Venkateswara Rao and S. D. Bhagat, Synthesis and physical properties of TEOS-based silica aerogels prepared by two step (acid–base) sol–gel process, Solid State Sci., 2004, 6, 945–952, DOI: 10.1016/j.solidstatesciences.2004.04.010.

59 A. Darmawan, R. Utari, R. E. Saputra, Suhartana and Y. Astuti, Synthesis and Characterization of Hydrophobic Silica Thin Layer Derived from Methyltrimethoxysilane (MTMS), IOP Conf. Ser.: Mater. Sci. Eng., 2018, 299, 012041, DOI: 10.1088/1757-899X/299/1/012041.

60 M. Mao, et al., Facile and green fabrication of flame-retardant $Ti_3C_2T_x$ MXene networks for ultrafast, reusable and weather-resistant fire warning, Chem. Eng. J., 2022, 427, 131615, DOI: 10.1016/j.cej.2021.131615.

61 Z.-H. Wu, et al., Silane modified MXene/polybenzazole nanocomposite aerogels with exceptional surface hydrophobicity, flame retardance and thermal insulation, Compos. Commun., 2023, 37, 101402, DOI: 10.1016/j.coco.2022.101402.

62 H.-Y. Chen, et al., Self-Adhesive Polydimethylsiloxane Foam Materials Decorated with MXene/Cellulose Nanofiber Interconnected Network for Versatile Functionalities, Adv. Funct. Mater., 2023, 33, 2304927, DOI: 10.1002/adfm.202304927.

63 R. Swathi, J. Shanthi and K. K. Anoop, Superhydrophilic TEOS/PF-127 based antireflection coating for solar and optical applications, Opt. Mater., 2021, 118, 111246, DOI: 10.1016/j.optmat.2021.111246.

64 M. Nosonovsky and B. Bhushan, Superhydrophobic surfaces and emerging applications: Non-adhesion, energy, green

GPTMS Hybrid Aerogel Monoliths and Coatings by Sol-Gel Method: A Viable Remedy for Oil-Spill Cleanup, Chemistry-Select, 2018, 3, 2989–2997, DOI: 10.1002/slct.201702967.

engineering, *Curr. Opin. Colloid Interface Sci.*, 2009, **14**, 270–280, DOI: **10.1016/j.cocis.2009.05.004**.

65 C. G. J. Prakash and R. Prasanth, Approaches to design a surface with tunable wettability: a review on surface properties, *J. Mater. Sci.*, 2021, **56**, 1–28, DOI: **10.1007/s10853-020-05116-1**.

66 A. Venkateswara Rao and D. Haranath, Effect of methyltrimethoxysilane as a synthesis component on the hydrophobicity and some physical properties of silica aerogels, *Microporous Mesoporous Mater.*, 1999, **30**, 267–273, DOI: **10.1016/S1387-1811(99)00037-2**.

67 B. Arkles, *Paint & Coatings Industry magazine 6*, Gelest Inc, Morrisville, PA, 2006.

68 X. Zeng, G. Xu, Y. Gao and Y. An, Surface Wettability of (3-aminopropyl)triethoxysilane Self-Assembled Monolayers, *J. Phys. Chem. B*, 2011, **115**, 450–454, DOI: **10.1021/jp109259b**.

69 Y. Zhou, *et al.*, A modified TA-APTES coating: Endowing porous membranes with uniform, durable superhydrophilicity and outstanding anti-crude oil-adhesion property via one-step process, *J. Membr. Sci.*, 2021, **618**, 118703, DOI: **10.1016/j.memsci.2020.118703**.